Compositional Variability and Mutation Spectra of Monophyletic SARS-CoV-2 Clades

Xufei Teng[1,2,3,#], Qianpeng Li[1,2,3,#], Zhao Li[1,2,3,#], Yuansheng Zhang[1,2,3,#], Guangyi Niu[1,2,3], Jingfa Xiao[1,2,3], Jun Yu[1,2,3,*], Zhang Zhang[1,2,3,*], Shuhui Song[1,2,3,*]

[1] *China National Center for Bioinformation, Beijing 100101, China*

[2] *National Genomics Data Center & CAS Key Laboratory of Genome Sciences and Information, Beijing Institute of Genomics, Chinese Academy of Sciences, Beijing 100101, China*

[3] *University of Chinese Academy of Sciences, Beijing 100049, China*

[#] These authors contributed equally

*Correspondence:
songshh@big.ac.cn (Song S), zhangzhang@big.ac.cn (Zhang Z), junyu@big.ac.cn (Yu J).

Abstract

COVID-19 and its causative pathogen SARS-CoV-2 have rushed the world into a staggering pandemic in a few months and a global fight against both is still going on. Here, we describe an analysis procedure where genome composition and its variables are related, through the genetic code, to molecular mechanisms based on understanding of RNA replication and its feedback loop from mutation to viral proteome sequence fraternity including effective sites on replicase-transcriptase complex. Our analysis starts with primary sequence information and identity-based phylogeny based on 22,051 SARS-CoV-2 genome sequences and evaluation of sequence variation patterns as mutation spectrum and its 12 permutations among organized clades tailored to two key mechanisms: strand-biased and function-associated mutations. Our findings include: (1) The most dominant mutation is C-to-U permutation whose abundant second-codon-position counts alter amino acid composition toward higher molecular weight and lower hydrophobicity albeit assumed most slightly deleterious. (2) The second abundance group includes: three negative-strand mutations U-to-C, A-to-G, G-to-A and a positive-strand mutation G-to-U generated through an identical mechanism as C-to-U. (3) A clade-associated and biased mutation trend is found attributable to elevated level of the negative-sense strand

synthesis. (4) Within-clade permutation variation is very informative for associating non-synonymous mutations and viral proteome changes. These findings demand a bioinformatics platform where emerging mutations are mapped on to mostly subtle but fast-adjusting viral proteomes and transcriptomes to provide biological and clinical information after logical convergence for effective pharmaceutical and diagnostic applications. Such thoughts and actions are in desperate need, especially in the middle of the *War against COVID-19*.

KEYWORDS: SARS-CoV-2; Nucleotide composition; Mutation spectrum; Viral replication

Introduction

COVID-19, a novel pneumonia epidemic causing an outbreak first identified and reported in Dec 2019 from China [1] and subsequently spread to other countries swiftly, has been posing enormous professional, economic, and political challenges to global health services and hazardous control systems. As of 12 June 2020, there have been 7,410,510 confirmed cases and 418,294 deaths reported [2]. COVID-19 is of great contagious (even at incubation period) and has lower mortality to our current understanding [3-5]. The novel betacoronavirus identified through *de novo* sequencing from patients with COVID-19 is designated as "Severe Acute Respiratory Syndrome Coronavirus 2 (SARS-CoV-2)" by International Committee on Taxonomy of Viruses (ICTV) [1, 6, 7].

The recent threats from SARS-CoV-2, SARS-CoV, and MERS-CoV are different from those of earlier human coronaviruses (CoVs), including alphacoronaviruses, such as hsa-CoV-229E, hsa-CoV-NL63, hsa-CoV-OC43 and hsa-CoV-HKU1 [8-10], in at least two aspects. First, the recent groups of betacoronaviruses appears to come more frequently in the past two decades as compared to the early comers where new members may be discovered as technology become more efficient and accurate [11]. The current SARS-CoV-2 is also different from both SARS-CoV and MERS-CoV as its genome composition is most closely for "living with mammals and humans", where a much lower G+C content has been evolved and is closer to two other human-adapted CoVs, hsa-CoV-229E and hsa-CoV-OC43, than its members of the recent group, although it shares higher sequence identities with the two new CoVs, 80.12% and 60.06%, respectively [11]. Second, it has been infecting far larger populations, as compared to the two recent outbreaks, with variable yet more complex symptoms [12]. The causative factors of such an unprecedented disease potency remain to be elucidated for the days and months to come [1, 3–7].

Genomes of coronaviruses mutate in a unique way where signatures of DNA pairing and repairing mechanisms are absent completely, and instead, they possess an error-prone synthesis of single-stranded full or partial genomic sequences by multi-component membrane-associated enzymatic structure known as the replicase-transcriptase complexes (RTCs) and double-membrane vesicles (DMVs) although they do have certain enzymatic activity resembling repair mechanisms of cellular organisms, such as proofreading [13], and other possible cellular mechanisms may also be involved, such as RNA editing as recently proposed [14,15]. Here we define a series of displays to understand compositional dynamics or variability that ultimately interconnects to proteomic variability including RTCs and DMVs (of course also other omics) through the organization of the genetic code [16–19]. We subsequently compare SARS-CoV-2 with other human CoVs for between-population variation analysis to point out that it is not a direct descendant of the previous human-infecting CoVs. We finally make efforts to decipher the SARS-CoV-2 clades for its variations and suggest that what we have seen now are not the natural picture of the pandemics and the missing-links are not among human populations but the wildlife close to human habitats in Southeast Asian territories, including islands and shorelines, not just limited to bats and pangolins. We also show how to examine clade-associated permutation variations and relate genetic variations to protein structures and phenotypic data. Nailing down a single animal of human origin of the virus will not be the goals of this genomics-based study but to provide information for smarter drug design, effective vaccine development, accurate diagnostics.

Results and Discussion

Compositional dynamics and its parameters are essential and useful features for evaluating the evolutionary status and molecular mechanisms of SARS-CoV-2 towards pandemics

RNA genomics is very different from DNA genomics in several ways [11]. First, in the RNA genome, the A:U basepair is actually 2 Daltons heavier than that of the G:C basepair due to a larger molecular weight of uridine, whereas in the DNA genome the GC pair is a single Dalton heavier than that of the A:T basepair. In CoVs, the G+C content is actually in a trend of reducing so that the virus is in turn becoming heavier due to the increased U content [11]. Second, single-stranded RNA genomes are synthesized without stable double-stranded

98 intermediates that allow mismatch repair albeit existence of short and extremely rare double-
99 stranded RNA fragments involved in interference-based immunity [20, 21]. Third, the
100 existence of Wobble basepairing for secondary structures is of essence for operational
101 functions of all RNA molecules in addition to genetic information inheritance [22]. That said,
102 we can now look at how the RNA genome of SARS-CoV-2 and related CoVs take advantage
103 of these RNA-centric features.

104 As a positive-sense single-stranded RNA virus, SARS-CoV-2 has a genome length of ~
105 29903 nucleotides (nt) (GenBank: NC_045512.2). It encodes two large polypeptides, ORF1a
106 and ORF1b, along with other 15 non-structure proteins (nsps; **Figure 1**A). In order to propagate
107 and complete the life cycle, its positive-sense genome is first replicated to synthesize full-
108 length negative-sense antigenomes and 10 shorter subgenomes (sgRNAs), executed by RTCs
109 and DMVs, and the sgRNAs encode four structural proteins (S, spike; E, envelope; M,
110 membrane; and N, nucleocapsid) and six accessory proteins (ORF3a, ORF6, ORF7a, ORF7b,
111 ORF8, and ORF10) arranged among structural proteins depending on the current annotation
112 (GenBank: NC_045512.2).

113 Traditionally, we use three basic plots to display composition dynamics based on primary
114 genomic parameters over genome length: G+C contents at three codon positions (GC1, GC2
115 and GC3); purine content (A+G content); and GC skew (the content of (G-C)/(G+C)). Here,
116 we use a 300-nt sliding window with a step size of 21 nt, as the majority of viral sequences are
117 protein-coding, to illustrate the dynamics of the composition parameters, G+C and purine
118 contents (Figure 1B). The G+C content of SARS-CoV-2 varies in a narrow but significant
119 window of 18.00% (31.67%–49.67%) and the purine content in a slightly narrower window of
120 15.50% (41.67%–57.17%) in average over the entire genome length. The GC skew of the
121 SARS-CoV-2 genome indicates the G+C ratio is relatively higher in structural proteins than
122 ORF1ab and this imbalance is a signature of distinct mutational biases caused by viral
123 replication machinery, known as RTCs. It is also variable as a frequent shift toward negative
124 values are often seen in individual ORFs and defined proteins. Such minor anomalies suggest
125 either recombination or selection events, which are species- or isolate-specific. The differences
126 become obvious when SARS-CoV-2 is compared to the closely-related bat and pangolin CoVs
127 (raf-betaCoV-RaTG13 and mja-betaCoV-P4L; Figure S1A and S1B), and the authentic within-
128 species variation is exemplified when SARS-CoV and MERS-CoV are matched up with civets
129 and camels in similar parameters, respectively (Figure S1C, S1D, S1E and S1F). The G+C
130 content of different codon positions is also very informative, where GC3 is very characteristic
131 of mutation pressure as it is obvious that all GC3 values of the viral proteins are biased toward

132 lower G+C contents. GC3-associated mutations often reflect directional mutation patterns as
133 observed strongly in certain lineages of plants and warm-blooded vertebrates as negative
134 gradients from the transcription starts, and such trends are attributable to a special DNA repair
135 mechanism, transcription-coupled DNA repair [23–25]. The notion here is to remind ourselves
136 that transcription-centric mutations may be accounted for some of the mutation events in RNA
137 viruses in their replication-transcription processes. Occasional twists from the trend often
138 indicate selective pressures, such as in the case of S, M, and N proteins, and weaker GC3 or
139 stronger GC1 or GC2 selections. Codon-associated G+C content trends are less informative for
140 small ORFs, such as the case of ORF10. Most of the sequence signatures are indicative rather
141 than proven functional relevance of proteins but very useful for providing clues of sequence
142 anomaly.

143 For studying RNA viral genomes, in addition to previously-defined parameters, we need to
144 introduce the concept of single nucleotide (A, U, G and C) contents at three codon positions
145 (such as U1, U2 and U3 for uridines) (**Figure 2**) and to plot out compositional dynamics for
146 positive-sense or the genome and negative-sense strands, which include both templates for
147 synthesizing new positive-sense genomes or antigenome and subgenomes. All viral mRNAs
148 are transcribed from an antigenome and other 9 subgenomes (Figure 2B). For compositional
149 dynamics of RNA genomes, uridine is the star nucleotide, and A+U content becomes the most
150 important. Just for the sake of convenience, we would like to keep the concept of G+C content
151 since it has been known to be a useful variable for DNA compositional dynamics [26] and
152 provide an approximation for less selected nucleotide position. For both DNA and RNA viruses,
153 this variable G+C content remains similar to their hosts mostly, except those that are not well
154 adapted to their hosts, such as SARS-CoV or MERS-CoV (Figure S2A; [11]).

155 As shown in a phylogenetic tree constructed based on 15 representative coronaviruses
156 (Figure 2A), the nucleotide content of SARS-CoV-2 is most similar to those of raf-betaCoV-
157 RaTG13 and mja-betaCoV-P4L, which are considered to be distantly related but most closely
158 related so-far-found host of SARS-CoV-2. Other known zoonotic and corresponding human
159 counterpart CoVs are rather close to each other in their compositions. We have made a few
160 interesting observations here. First, the single nucleotide content is more informative than G+C
161 content, especially for genome analysis on RNA viruses. The former points out only how G+C
162 content drifts toward richness or poorness but the latter narrows it down to single nucleotide
163 effect. In our case, U stands out at cp3, which alters the overall nucleotide contents, and it
164 drives the G+C content so low that even its partner A content has gone to the same extremity,
165 so that the low G+C content is a result of both lowering U and A. If the organization principles

166 are considered here, half of the codons are not sensitive to cp3 changes, and most of them are
167 smaller amino acids (Figure S2B; [16–19]). Second, at the cp1, G and C contents are both
168 pulled apart toward extremity but not A or U, while the two pyrimidines and two purines appear
169 stretched to separate directions; these trends suggest strong selective pressure at the first codon
170 position over the entire genome. It is indeed that cp1 codons shoulder the most mutation
171 pressures since they fall into all 4 negative-sense strand permutations (known as R1-derived
172 permutations, C-to-U, G-to-A, U-to-C and A-to-G). Third, the cp2 contents are most row-
173 flipping changes referenced to the genetic code organization [18]. These alterations are very
174 useful for alternating chemical characteristics between related amino acids, and in terms of
175 flexibility, cp2 codons are less stringent than cp3 but more flexible than cp1. The balancing
176 power becomes more obvious when ORFs or proteins are examined individually for their
177 composition dynamics (Figure 1C). Finally, it is conclusive that the more similar the CoVs in
178 composition dynamic parameters, the closer they are genetically and phylogenetically in
179 principle. However, primary parameters, such as G+C and purine contents are necessary but
180 may not be sufficient. For instance, there has been a CoV genome isolate from a wild vole
181 captured in northeastern China, whose G+C and purine contents overlap with SARS-CoV-2
182 completely (Rodent coronavirus isolate RtMruf-CoV-2/JL2014; 0.38, 0.496; [27]) but its
183 genome sequence is different (sharing 61.87% identity with SARS-CoV-2). Therefore, we have
184 yet to find a within-population immediate animal host of SARS-CoV-2 albeit best similarity
185 of composition dynamics seen among them.
186 Our subsequent study is focused on composition dynamics within CoV genomes. It is
187 interesting to see uniformity among all codon position contents of all CoV genomes, increased
188 G+C content from antigenomes to subgenomes. However, this trend is an illusion where the
189 real trend is the lower G+C content of antigenomes but higher G+C contents of subgenomes
190 due to stronger selection over structural proteins. This observation becomes clearer when all
191 ORFs and proteins are scrutinized one by one (Figure 1C and Figures S1). SARS-CoV-2 has
192 an exceptionally short subgenome 9 (sg9) which only contains ORF10, but we have no
193 evidence that it is either functional or non-functional. These results collectively remind us that
194 SARS-CoV-2 and its two most-closely-related CoVs, unlike in the case of many other known
195 CoVs, have a unique genome composition and similar dynamics to the early-adapted human
196 CoVs [11], and CoV-borne bats and other mammals may already coexist with ability to jump
197 on to humans and domestic animals but only limited by environmental and geographic
198 constraints.
199

Mutation spectrum is composed of permutations that are distinct according to their strand specificity, order of synthesis, and ratio of positive-sense vs. negative-sense strands during propagation

We use 12 permutations to represent directional mutations and classify them according to strand-specific replication mechanisms (**Figure 3**) since they are readily related to codons [11] (Figure S2B). From a total of 5,054 point mutations, 1,416, 1,497, and 2,141 mutations fall on codon position 1, 2, and 3, respectively. The permutations are categorized into R1 (C-to-U, G-to-A, U-to-C and A-to-G), R2 (C-to-A, U-to-G, A-to-C and G-to-U), and R12 (C-to-G, U-to-A, A-to-U and G-to-C) derived according to their occurrence tailored to RTC-directed strand synthesis: R1 from the first negative-sense strand, R2 from the subsequent positive-sense strand, and R12 from R1 plus R2. The most abundant permutations are four R1 permutations and one R2 permutation, G-to-U (Figure 3A and 3B). What have we shown here is how sensitive are nucleotide content of cp3 to selective pressure, and most cp3 permutations disappear except the R2 G-to-U permutations at cp3, where all changes are transversions and more than half of all codons (all pro-diversity changes) are sensitive to them. Similar results are observed in our analysis on SARS-CoV and MERS-CoV (Figure S3A and S3B). There are slightly different patterns among SARS-CoV and MERS-CoV and their within-population mammals from the SARS-CoVs and close relatives, the higher U-to-C permutations. The predominate C-to-U represents a driving force of variation, and it manifests why both G+C and A+G contents of SARS-CoV-2 appear relatively lower against MERS-CoV and SARS-CoV and even more when compared to human CoVs, such as 229E and OC43 (Figure S2A).

Since most cp1 and cp2 related permutations are sensitive to selection, we have examined how individual permutations correlated to codon rearrangements in the two halves tables: pro-diversity and pro-robustness (Figure 3C and 3D) [16, 17]. Only two examples, C-to-U and A-to-G, are shown here and the rest are summarized in Figure S3C. Several observations are worthy of in-depth discussion. First, it is known that three amino acids and their codons are unique in balancing one of two purine-sensitive halves; they are Leu (leucine), Arg (arginine), and Ser (serine) [16–19]. The most abundant amino acid in protein coding sequences (known as codon usage) is Leu and it buffers C-to-U|U-to-C mutations at cp1. Arg and Ser are also abundant as they both are 6-fold degenerate codons; Arg appears buffering A-to-G|G-to-A at cp1 and Ser carries two: U-to-A|A-to-U at cp1 and G-to-C|C-to-G at cp2. Second, amino acid exchanges are permissive in physiochemical properties [23–25]. For instance, Ser has a very similar size to Ala (alanine) so that G+C content increase is buffered by the two amino acids as G-to-U|U-to-G permutations. Third, other examples are codon alterations among

234 hydrophobic amino acids as they are mostly C-to-U changes at cp2 among those in the pro-
235 robustness half. The overall effects are displayed together in Figure 3D. It is rather clear that
236 changes toward lower G+C content and near the balanced purine content are both beneficial
237 for CoVs, especially SARS-CoV-2, as these changes are pro-diversity, in favor of larger and
238 more hydrophilic amino acids.
239
240 **Clade-associated biased mutation trend in SARS-CoV-2 revealed physiochemical**
241 **features of replication machinery**
242 Difficulties for analyzing CoV genomes are multifold. Since we have yet to identify the natural
243 hosts and mammalian intermediate hosts, if there is any, this massive dataset has to be analyzed
244 by stratifying the data into structured and non-structured clades; the former can be analyzed
245 first and the rest await further ideas. The next is even more troublesome. Assuming that we
246 have 5 or more genome sequences per CoV isolate and variations identified among them are
247 still a miniscule fraction of the total virions produced in a patient body (medians and means of
248 variations per CoV isolate among C01 to C09, see Table S3), since the viral load per patient
249 sample, such as sputum [28, 29], is equivalent to a 5-person or more sampling of the entire
250 human population on earth, 1 out of 10^9. Even so, we have still been able to find shared
251 variations among patient samples occasionally and even more lucky to have some clade
252 structures, by and large due to the relatedness of the patients in the transmission network.
253 Finally, we have to admit that many assumptions have to be made about these samples and
254 their genome sequences above sequence and assembly errors for phylogeny and genetic studies.
255 Nevertheless, we have constructed a somewhat stable phylogenetic tree-and-branch
256 structure for further analysis (**Figure 4**A). It is composed of 8 monophyletic clades and 1 non-
257 monophyletic clade based on both orders of sample collection date and highly-shared mutations.
258 Among the clades, C02 shares two landmark mutations, C8782U in ORF1ab and U28144C in
259 ORF8, and earlier date (2019/12/30). C04 shares three more mutations (C17747U, A17858G,
260 and C18060U in ORF1ab) than what C02 have, and a late collection date (2020/02/20). Clades
261 C03, C05, and C07 are also distinguishable by some major mutations, so are C06, C08, and
262 C09; the latter clades are clustered together based on four shared and other clade-associated
263 mutations. The leftover large number of isolates that lack all landmark mutations are grouped
264 into C01, which have the earliest collection date on 2019/12/24. According to the literature and
265 our discussion, we have further grouped the clades into three clusters, S (C02 and C04), G
266 (C06, C08 and C09), and L (all the rest) since phylogeny shows clear divergence among them.
267 We have several notions about this imperfect hierarchical structure. First, our within- and

268 between-clade analysis of high major allele frequency (MAF) variations reveals that some
269 clade-associated signature mutations are also shared among clades. For instance, C14805U in
270 ORF1ab and A24034G in Cluster S have recurred in other clades of different clusters, which
271 are excellent landmarks for subclade definition. Another notion is that higher MAF within-
272 clade mutations (such as MAF>0.2) are mostly non-synonymous mutations, indicating
273 selection at work (Figure S4). Our neighbor-joining tree based on distances from 9 clades
274 suggests that SARS-CoV-2 appears originated from multiple zoonotic reservoirs instead of a
275 single direct ancestor (Figure S4). In addition, our classification rationales are largely in
276 agreement with published reports [30]; for example, Cluster S is in accordance with previously
277 defined S type [31] and Cluster G is in line with GISAID [32] defined the G clade. Cluster L
278 is similar to the V and L clades combined, of GISAID. A maximum likelihood (ML) based
279 unrooted phylogenetic tree is shown in Figure 4B.

280 To look for clade-associated compositional and functional features, we have first built a
281 consensus sequence for each clade and subsequently calculated frequencies for each within-
282 clade permutation (Table S2; **Figure 5**A and 5B). A key assumption behind this is that certain
283 functional mutations may have clade-specific effects on mutation spectrum, to close a loop
284 where sequence mutations through genetic coding principles alter the viral proteome function.
285 Our observations are of importance in establishing logics about compositional dynamics
286 between nucleic acids and proteins. First, permutations among clades are indeed variable
287 according to their proportions calculated from genome variants, and aside from 5 high-
288 proportion permutations, 4 R1 and 1 R2 permutations, two other R2 and one R12 permutations
289 appear also joining in, which are U-to-G and A-to-C, as well as A-to-U, respectively. Second,
290 the variable permutations, where some may represent effect of mutation pressure and others
291 may exaggerate selection pressure, are unique to clades and clade clusters. For instance, clade
292 cluster S has the lowest G-to-U fraction as compared to those of L and G; in addition, among
293 the S clades, C04 has the lowest value of G-to-U. Similarly, C03, C05, C06, C08, and C09
294 have relatively higher G-to-U permutations. Third, based on the disparity of permutations or
295 simply mutation spectra, we have taken a rather radical step to assume RTC statuses in favor
296 of either *tight* or *loose* statuses for binding to purines and pyrimidines (see Figure S5). Since
297 purines are larger than pyrimidines in size, the purine- or R-tight must be different from
298 pyrimidine- or Y-tight. The results are strikingly predictable in that the R-tight status suggests
299 a tighter binding pocket where a descending trend for tight permutations (C-to-U, G-to-U, and
300 U-to-A) reverses into the opposite trend for Y-tight permutations. It indicates that the RTC
301 structure and conformation variables may be definable in principle. At this point, we do not

302 have discrete definitions for these so-called tight statuses but the less trendy R-loose and Y-
303 loose statuses also support a similar idea.
304 We have further examined the compositional subtleties among the clades and clusters with
305 a focus on G+C and purine content variability as both contents appear drifting toward optima
306 in SARS-CoV-2 and its relatives (Figure 5C and 5D). Different clades exhibit distinct
307 compositional features and such dynamics are very indicative for the existence of feedback
308 loops connecting RNA variables to protein variables. Two directions have to be advised for
309 understanding these features albeit in absence of between-clade statistics. The first direction is
310 driven by strong mutations, perhaps coupled to tight-loose switches in the catalytic pocket of
311 RdRPs in RTCs. It is clear that except C01, the G or C06-C08-C09 cluster has the lowest G+C
312 (0.37929, based on a C08 CoV sampled in Australia) and the lowest purine contents (0.49527,
313 based on a C08 CoV collected in Bangladesh and a C09 CoV collected in England). Both lower
314 G+C and purine contents are indicative of mutation pressure and signal this fast-evolving
315 cluster of CoVs. Since this cluster has the largest collection of CoVs, it is also not surprising
316 to see a more complex median diversification within clades (Figure 5C and 5D). The second
317 direction is the drive from selection or both selection and mutation in balance or imbalance, as
318 well as in modes of fine-tuning or quick-escaping. Some results from our analyses are shown
319 here for briefing purposes (Figure 5E to 5G). For instance, G+C and purine contents at cp3 are
320 informative for mutation drives and other measures are less clear cut (Figure 5F), given the
321 evidence that even MAFs among clades are not stably distributed among clades as lower MAF
322 variations are rather sporadic and hard to analyze even binned into groups (data not shown).
323 Based on our clade and clade cluster analysis, it is tempting for us to speculate that there
324 are plenty of rooms for further investigations into mutation spectra among large clades and
325 even smaller clades or closely related individual CoV genomes for several reasons. First, all
326 high-frequency MAFs should be identified and classified and these variations are candidates
327 for highly selected mutations. Second, all within-clade minor but not rare alleles (less than
328 1/10,000), such as those of MAFs in a range of 0.01% to 10% should also be identified; they
329 provide basis of within-clade sequence analysis. Third, all non-structured CoV genomes must
330 be also classified based on shared variations, as they are not only valuable for within-clade but
331 also for clade-cluster analyses since there is a large background of genome variations not yet
332 brought into the databases.
333
334 **Within-clade variations and their implications for future SARS-CoV surveillance**

335 Within-clade compositional dynamics can also be very informative, especially for covering
336 and predicting future functional changes, such as identifying mutated and diversified forms of
337 CoVs for drug and vaccine designs. It is also of essence for nucleic acid-based diagnostics,
338 such as clade-specific identifications. We are in a process of developing an interactive database
339 and mutation-function predicting algorithms based on our results to interpret novel sequence
340 variations in real time. Within-population variations are identified based on clade consensus
341 sequence after alignment and extracted from datasets that have hundreds and thousands of
342 genome sequences. The analysis of within-population variations relies on structured phylogeny
343 and proportion change of permutations. The changes, based on functional relevance, can be
344 classified into either copy number-related or RTC-specificity related, or sometimes both.
345 We have taken two steps to extract information in order to distinguish the underlining
346 mechanisms (**Figure 6**). In the first approach, we identify key mutations based on MAF of
347 mutations with a consideration of relatively even distribution among subclades and name the
348 subclades in a sequential order based on the absence of a subset (Figure 6A). In the second step,
349 we plot out permutations to track changes among subclades (Figure 6B). For instance, clade
350 C02 can be divided into 8 subclades and its variable permutation fractions are clearly
351 recognizable. An immediate discovery is the trends of descending C-to-U, ascending A-to-G,
352 and wavy G-to-U that initially goes up with A-to-G but rides down with C-to-U afterward.
353 Taking the two smaller clades, such as C03 and C05, as examples (Figure 6D and 6E), we
354 first find that their trends of permutation variables show opposite directions, where the
355 increasing C-to-U accompanies with the decreasing G-to-U. A closer examination reveals that
356 the increasing C-to-U in C03 is also accompanied by descending U-to-C. The only permutation
357 showing an increasing trend in C03 is G-to-A. The take-home message from these trends is
358 that RNA synthesis of this subclade is biased toward producing more negative-sense strands
359 or its mutation spectrum exhibits increasing mutations generated during the negative-sense
360 strand synthesis. Such analysis can be carried out continuously when more CoV genome data
361 become available as other within-clade variations are not as informative as C03 vs. C05 (Figure
362 S6).
363 Several precautions are worth noting in such analysis. The most noticeable weakness is the
364 fact that we assume function-related mutations are discovered in our dataset. As we have
365 proposed an analogy before, chances are slim, dozens out of millions or even billions.
366 Furthermore, even if we see drastic changes in permutations and mutation spectra, the
367 mutations we identified still need validation empirically and based on different data types or
368 sources albeit rare and precious. Finally, most frequently encountered situations are those that

369 multiple mutations exhibit cofounding effects for a phenotypically identified functional or
370 structural feature, and undoubtedly, more and deep-sequencing data are still invaluable and
371 irreplaceable.
372

373 ## Conclusion

374 This COVID-19 pandemic provides once-in-a-lifetime opportunity for the fields of
375 biomedicine and other life sciences to work together on it as many facets as possible albeit
376 exchanging with lives and other massive losses. If lessons told, we had learned things in serious
377 ways in the last two CoV epidemics and we did prepare ourselves with vaccines and medication
378 since, we would not have suffered this much this time. If one assumes that the last two
379 outbreaks of SARS-CoV and MERS-CoV came surely by chances, this time SARS-CoV-2 is
380 here for real, and a worst-case scenario is that it may stay with us forever or until effective
381 vaccination is developed. Nevertheless, it certainly will stay with us for quite a while for many
382 reasons [11]. First, at least it and other within-population versions of coronaviruses will
383 definitely come again because we have not been able to trace its origin and ways its
384 transmission from the very beginning, neither the Wuhan outbreak nor the recent Beijing
385 outbreak in China even guided with very strict quarantine roles and prompt action plans. Next,
386 this particular virus, SARS-CoV-2, has evolved to a composition status where some of its
387 natural yet genetically distant hosts or possible intermediate mammalian hosts have acquired
388 similar status [33, 34]. Furthermore, we do not yet have enough data to really map out the
389 phylogenetic position that allows us to pinpoint its natural origin and human transmission
390 routes.

391 The number one needs for us is data, genomic and clinical data, which should be as
392 complete as possible and with characteristics including high-quality and high-coverage at
393 single-molecule resolution. We currently have been acquiring genomic data and the specialized
394 databases have collections over ten thousand non-redundant sequence variations, but still not
395 enough to address more than a few possible functional changes of some key protein
396 components [35–38], let alone understanding mutation-centric cellular mechanisms. Based on
397 median and mean estimates, we have on average a mutation accumulation rate of half a dozen
398 per patient. Although there have been data reported from single-molecule sequencing platform
399 but they are low in coverage [39].

400 Our final notion is to emphasize the importance of analysis strategies and supporting
401 platforms. Since questions always overwhelm what we can possibly address [40], prioritizing

402 tasks are of essence together with choices of strategies. The first platform to be established
403 concerns mutation-to-function interpretation, where we have present one in this report. Another
404 to be considered is mathematic modeling, such as cellular and disease transmissions [41–46]
405 and viral mutation-selection paradigm, for testing and evaluating different parameters and
406 prioritizing what kind of data to be acquired with high priorities. In addition, cellular and
407 molecular data, including different omics studies [47], all need to be incorporated into a
408 COVID-19 knowledgebase, where information from multi-disciplinary studies are managed,
409 organized, and mined.
410

411 ## Materials and Methods

412 **SARS-CoV-2 and other related coronaviruses sequences**

413 We used the public-available SARS-CoV-2 data collected worldwide among the major
414 databases, including CNCB/NGDC [48], CNGBdb [49], GISAID [32], GenBank [50] and
415 NMDC [51] on June 12th, 2020. To ensure authenticity and reliability, our datasets must meet
416 the following criteria: (1) The genome sequence is labeled as complete that covers all coding
417 regions of the reference genome (GenBank accession NC_045512.2). (2) It has no more than
418 15 uncertain bases that often substituted as "N"s. (3) It has no more than 50 degenerate bases
419 that often labeled as discrete nucleotides. These high-quality genomes were aligned to the
420 reference using MUSCLE (version 3.8.31) with default parameter settings [52]. Further
421 analyses of SARS-CoV-2 and related CoV genomes are referenced to genome annotation of
422 the same reference genome (NC_045512.2) and other information provided by the RefSeq
423 database at NCBI.

424 Other closely related CoV genome sequences used include hsa-betaCoV-HKU1, hsa-
425 betaCoV-OC43, ave-gamaCoV, mga-gamaCoV, smu-alphaCoV-WS, hsa-alphaCoV-229E,
426 hsa-alphaCoV-NL63, taf-alphaCoV-NL63, MERS-CoV (from human and camel hosts), cdr-
427 betaCoV-B73, SARS-CoV (from human and civet hosts), pla-betaCoV-SZ3 and raf-betaCoV-
428 RaTG13 are retrieved from NCBI and mja-betaCoV-P4L are retrieved from NGDC. A full
429 listing of our sequences dataset including virus genre, strain name, accession number and
430 sources is provided in Table S3.
431

432 **Calculation of genomic composition parameters**

433 We display several genomic composition dynamics and its parameters (G+C content, A+G
434 content and GC skew) using different sliding windows. The first 300 nt are grouped as an initial

435 window, and subsequent windows are uniformly shifted in a 21-nt step. Within these displays,
436 the G+C contents referenced to the three codon positions of each open reading frame or ORF
437 are measured by adjusting the sliding window according to the ORF lengths within viral
438 genomes. As for ORFs longer than 2000 nt, a relatively large window size (300 nt) is adopted,
439 and the step size is calculated via a custom formula $round\left(\frac{length_{ORF}-300}{600}\right)-vb,\ 0 \leq vb \leq 2$
440 where $length_{ORF}$ denotes the length of ORF and vb varied from zero to two bases to make
441 sure the window size is divisible by 3; for ORFs with a medium size (longer than 500 bases
442 and shorter than 2000 nt), the window size is defined as $round\left(\frac{1}{4} * length_{ORF}\right)-vb,\ 0 \leq$
443 $vb \leq 2$, while the step size is simply defined as 3 nt; as for those small ORFs (shorter than 500
444 nt) such as structural proteins, a constant 21-nt window size and 3-nt step size is used for
445 calculating genomic composition frequency.

446 The criteria for choosing the representative CoV genome sequences for constructing a
447 representative phylogenetic tree (Figure 2) are multi-fold. First, we include all 7 human-
448 infecting coronaviruses for the analysis, which are SARS-CoV, SARS-CoV-2, MERS-CoV,
449 hsa-alphaCoV-229E, hsa-betaCoV-OC43, hsa-betaCoV-HKU1, and hsa-alphaCoV-NL63 (a
450 prefix hsa- standing for *Homo sapiens* was used to label the unfamiliar human-infecting CoVs).
451 Second, we categorized all human-infecting, for simplicity, into 4 lineages: SARS-CoV-2,
452 SARS-CoV, MERS-CoV, and the older human CoV lineages. Therefore, their related CoVs in
453 the literature were also selected for the analysis, including a single closely-related CoVs for
454 each lineage (based on sequence identity): SARS-CoV-related (pla-betaCoV-SZ3), MERS-
455 CoV-related (cdr-betaCoV-B73), SARS-CoV-2 related (raf-betaCoV-RaTG13), and NL63-
456 related (taf-alphaCoV-NL63; both species and CoV genera were labelled for clarity). Third,
457 we also added more informative CoV genome sequences to enrich lineage-associated
458 information, which are a pangolin coronavirus genome (mja-betaCoV-P4L) reported to be
459 closed to SARS-CoV-2 and 3 non-beta-coronaviruses that infect animals (e.g., ave-gamaCoV
460 from gamma-coronavirus genus and smu-alphaCoV-WS from alpha-coronavirus genus).
461 Fourth, we only used complete protein-coding sequences from the CoVs to construct the
462 phylogenetic tree and to calculate genome parameter contents. The sequences were aligned by
463 using MUSCLE and the UPGMA tree was constructed by using MEGA-X [53]. The G+C
464 content and single nucleotide content of each virus genome at three codon positions was also
465 calculated. Subgenomes of SARS-CoV was obtained from Marra et al [54], and we annotated
466 the subgenomes of SARS-CoV-2, mja-betaCoV-P4L, and raf-betaCoV-RaTG13 based on the
467 annotation of NCBI (GenBank accession NC_045512.2). In addition, G+C and single

468 nucleotide contents of the complete genome and its subgenomes of these four viruses at three
469 codon positions were displayed to serve as sequence composition references.
470
471 **Variation calling and categorization**
472 All sequence variations are identified and categorized based on comparisons between the query
473 and the reference genomes, and files were generated by using an in-hoc Perl scripts based on
474 alignment results. The tailored annotation (gene, location and consequence on the protein
475 sequence) of each variant is determined with VEP (version 99.0) [55]. Since a large number of
476 gaps and low-quality sequences at the 3' and 5' ends, variations (substitutions, insertions and
477 deletions or indels) occurring 50 nt each at 5'- and 3'-ends of the genome are not considered.
478 Since the higher quartile of variations per genome among SARS-CoV-2 populations is 9
479 (based on the 22,051 sequences we analyzed in this study), we filtered out the problematic sites
480 that exceed 50 variations as compared to the reference genome. CoV genome sequences have
481 at least one mutation are used in this study. A full listing of variations among coding regions
482 identified in this study is provided in Table S4.
483 All continuously updated mutation files of the SARS-CoV-2 populations in variant call
484 format (version 4.2) are deposited at the variation page of the 2019nCoVR database contributed
485 by CNCB/NGDC (https://bigd.big.ac.cn/ncov/variation/).
486
487 **Mutation spectrum analysis**
488 A mutation spectrum for within-population variations is composed of two lines of information;
489 one concerns mutations that are referenced to a population consensus built based on the entire
490 collection, and the other contains frequencies of all mutations and their directional changes,
491 i.e., permutations. To reduce pitfalls of sequencing errors, we only selected mutations that
492 occur more than twice in the whole collection of SARS-CoV-2 populations (clades or clade
493 clusters that are often defined based on phylogenetic analysis). In theory, there are 16 possible
494 permutations but 4 of them are unrecognizable so that 12 permutations (C-to-U, A-to-G, U-to-
495 C, G-to-A, G-to-U, U-to-G, A-to-C, C-to-A, U-to-A, G-to-C, C-to-G and A-to-U) are there as
496 an informative set. When the number of CoV genomes collected are limited, such as SARS-
497 CoVs and MERS-CoVs, entire data sets are pooled together without clades. In our analyses on
498 SARS-CoVs and MERS-CoVs (Figure S3A), we aligned sequences from these two lineages to
499 their reference genomes (SARS-CoV: NC_004718.3; MERS-CoV: NC_019843.3) to call
500 variations. When aligned on overlapping sequences, due to large deletions and additional ORFs,
501 are encountered, we always choose the largest or only one of the ORFs to represent the segment,

502 respectively. For example, in SARS-CoV lineage, if a mutation falls into the overlapping
503 region of ORF9a (encoding the N protein) and ORF9b, we have only used the ORF9a
504 annotations to avoid redundancy.
505
506 **Phylogeny constructing**
507 Given the scale of SARS-CoV-2 sequence collections, we focused on genomes with unique
508 information contributing to phylogenetic analysis. First, mutations (including single-nucleotide
509 substitution and indels) at frequencies equal or greater than 10 in between-clade or –population
510 calls were selected. FastTree (version 2.1.11) [56] is used to construct maximum likelihood
511 phylogeny based on 5,121 genomes that have met our criteria, and iTol [57], an interactive web
512 server was employed for setting an unrooted format and annotating samples.
513 For Figure S4, the neighbor-joining method is used for constructing phylogeny from the
514 Euclidean distance of the mutation frequency matrix of clades, and the tree was generated and
515 visualized by R package phangorn [58] and ggtree [59].
516
517 **Estimation of G+C and purine contents of genome sequences**
518 G+C and purine (or A+G) contents of CoVs in general vary in a narrow range, and therefore,
519 subtleties among the content changes have to be scrutinized with low-quality sequences
520 excluded. A more sensitive approach is used in this study where two points are assumed; all
521 genomes are full-length and variant alleles in coding sequences are the varied composition.
522 The absolute frequencies of A+G and G+C content are defined as:
523
524 $$Genomic\ AG\ content = \frac{8954 + 5492 + (A_{alt} - A_{ref}) + (G_{alt} - G_{ref})}{29903 - (Del_{alt} - Ins_{alt})} \quad (1)$$
525 and
526 $$Genomic\ GC\ content = \frac{5492 + 5863 + (G_{alt} - G_{ref}) + (C_{alt} - C_{ref})}{29903 - (Del_{alt} - Ins_{alt})} \quad (2)$$
527
528 where 8,954, 5,492, 5,863, and 29,903 are the frequencies of A, G, C and total length of the
529 SARS-CoV-2 reference, respectively. For any sequence compared with the reference, the
530 Del_{alt} and Ins_{alt} measures the deleted and inserted nucleotides of this sequence, respectively,
531 and that is why $(Del_{alt} - Ins_{alt})$ means the variation of sequence length. For all the variant
532 sites in this sequence, $(A_{alt} - A_{ref}) + (G_{alt} - G_{ref})$ in Equation (1) measures the number of
533 A and G variations in compared sequence, A_{alt} and G_{alt} denote the number of nucleotides

534 mutated to A or G while A_{ref} and G_{ref} represent the number of nucleotides mutated from A or
535 G. Similarly, $(G_{alt} - G_{ref}) + (C_{alt} - C_{ref})$ in Equation (2) represents the varied number of G
536 and C among compared sequences.
537
538 **Clade subgrouping**
539 To detect trend followers and disrupters in mutation spectra, a pipeline was developed to select
540 such genomes and mutations within clades iteratively. The first step includes locating high-
541 frequency mutations (major alleles, MA) in a clade and extracting all genomes without this
542 MA mutation to form a subset of the clade. The second step is, within the new subclade, to
543 iterate the process until such mutations are thoroughly identified and no more mutations exceed
544 a manually set threshold of MAF. Since the number of unique variations among clades have
545 been varying significantly over time, the thresholds are 0.05 in C01, C04, C06, C08 and C09;
546 0.1 in C02, C03, C05 and C07. The proportion of permutations in each subclade and the located
547 gene and mutation type (synonymous or non-synonymous) of mutations are provided in Table
548 S5.
549

550 ## Authors' contributions

551 JY designed, supervised, and coordinated the study. SS, ZZ and JX participated in the
552 design of the study. XT, QL, ZL, YZ, GN performed the data analysis. JY, SS, XT, QL, ZL,
553 YZ designed and drew the figures. JY and XT drafted the manuscript. JY, ZZ, SS, QL and
554 XT revised the manuscript. All authors read and approved the final manuscript.
555

556 ## Competing interests

557 The authors have declared no competing interests.
558

559 ## Acknowledgements

560 This work was supported by grants from The Strategic Priority Research Program of the
561 Chinese Academy of Sciences [XDA19090116 to S.S., XDA19050302 to Z.Z.], National Key
562 R&D Program of China [2020YFC0848900, 2017YFC0907502], 13th Five-year
563 Informatization Plan of Chinese Academy of Sciences [XXH13505-05], K. C. Wong Education
564 Foundation to Z.Z., and International Partnership Program of the Chinese Academy of Sciences
565 [153F11KYSB20160008]. The Youth Innovation Promotion Association of Chinese Academy
566 of Science [2017141 to S.S.]; Funding for open access charge: The Youth Innovation

Promotion Association of Chinese Academy of Science. We thank our colleagues and students for their hard working on the 2019nCoVR (https://bigd.big.ac.cn/ncov). We thank Dr. Lina Ma, Lili Hao, and Meng Zhang for useful suggestions and discussion of this manuscript.

References

[1] Wu F, Zhao S, Yu B, Chen Y-M, Wang W, Song Z-G, et al. A new coronavirus associated with human respiratory disease in China. Nature 2020;579:265–9.

[2] World Health Organization. Coronavirus disease (COVID-2019) situation report - 144. https://www.who.int/emergencies/diseases/novel-coronavirus-2019/situation-reports (Jun 12 2020, date last accessed).

[3] He X, Lau EHY, Wu P, Deng X, Wang J, Hao X, et al. Temporal dynamics in viral shedding and transmissibility of COVID-19. Nat Med 2020;26:672–5.

[4] Zou L, Ruan F, Huang M, Liang L, Huang H, Hong Z, et al. SARS-CoV-2 Viral Load in Upper Respiratory Specimens of Infected Patients. N Engl J Med 2020;382:1177-9.

[5] Wu Z, McGoogan JM. Characteristics of and Important Lessons From the Coronavirus Disease 2019 (COVID-19) Outbreak in China: Summary of a Report of 72314 Cases From the Chinese Center for Disease Control and Prevention. JAMA 2020.

[6] Coronaviridae Study Group of the International Committee on Taxonomy of Viruses. The species Severe acute respiratory syndrome-related coronavirus: classifying 2019-nCoV and naming it SARS-CoV-2. Nat Microbiol 2020;5:536–44.

[7] Zhu N, Zhang D, Wang W, Li X, Yang B, Song J, et al. A Novel Coronavirus from Patients with Pneumonia in China, 2019. N Engl J Med 2020;382:727–33.

[8] Cui J, Li F, Shi Z-L. Origin and evolution of pathogenic coronaviruses. Nat Rev Microbiol 2019;17:181–92.

[9] de Wit E, van Doremalen N, Falzarano D, Munster VJ. SARS and MERS: recent insights into emerging coronaviruses. Nat Rev Microbiol 2016;14:523–34.

[10] Fung TS, Liu DX. Human Coronavirus: Host-Pathogen Interaction. Annu Rev Microbiol 2019;73:529–57.

[11] Yu J. From Mutation Signature to Molecular Mechanism in the RNA World: A Case of SARS-CoV-2. Genomics Proteomics Bioinformatics 2020;in press.

[12] Guo Y-R, Cao Q-D, Hong Z-S, Tan Y-Y, Chen S-D, Jin H-J, et al. The origin, transmission and clinical therapies on coronavirus disease 2019 (COVID-19) outbreak - an update on the status. Mil Med Res 2020;7:11.

600 [13] Smith EC, Blanc H, Surdel MC, Vignuzzi M, Denison MR. Coronaviruses lacking
601 exoribonuclease activity are susceptible to lethal mutagenesis: evidence for proofreading and
602 potential therapeutics. PLoS Pathog 2013;9:e1003565.
603 [14] Simmonds P. Rampant C-->U Hypermutation in the Genomes of SARS-CoV-2 and Other
604 Coronaviruses: Causes and Consequences for Their Short- and Long-Term Evolutionary
605 Trajectories. mSphere 2020;5.
606 [15] Di Giorgio S, Martignano F, Torcia MG, Mattiuz G, Conticello SG. Evidence for host-
607 dependent RNA editing in the transcriptome of SARS-CoV-2. Sci Adv 2020;6:eabb5813.
608 [16] Xiao J, Yu J. A scenario on the stepwise evolution of the genetic code. Genomics
609 Proteomics Bioinformatics 2007;5:143–51.
610 [17] Yu J. A content-centric organization of the genetic code. Genomics Proteomics
611 Bioinformatics 2007;5:1–6.
612 [18] Zhang Z, Yu J. On the organizational dynamics of the genetic code. Genomics Proteomics
613 Bioinformatics 2011;9:21–9.
614 [19] Zhang Z, Yu J. The pendulum model for genome compositional dynamics: from the four
615 nucleotides to the twenty amino acids. Genomics Proteomics Bioinformatics 2012;10:175–80.
616 [20] DeWitte-Orr SJ, Collins SE, Bauer CMT, Bowdish DM, Mossman KL. An accessory to
617 the 'Trinity': SR-As are essential pathogen sensors of extracellular dsRNA, mediating entry and
618 leading to subsequent type I IFN responses. PLoS Pathog 2010;6:e1000829.
619 [21] Totura AL, Baric RS. SARS coronavirus pathogenesis: host innate immune responses and
620 viral antagonism of interferon. Curr Opin Virol 2012;2:264–75.
621 [22] Crick FH. Codon--anticodon pairing: the wobble hypothesis. J Mol Biol 1966;19:548–55.
622 [23] Cui P, Lin Q, Ding F, Hu S, Yu J. The transcript-centric mutations in human genomes.
623 Genomics Proteomics Bioinformatics 2012;10:11–22.
624 [24] Cui P, Ding F, Lin Q, Zhang L, Li A, Zhang Z, et al. Distinct contributions of replication
625 and transcription to mutation rate variation of human genomes. Genomics Proteomics
626 Bioinformatics 2012;10:4–10.
627 [25] Wong GK-S, Wang J, Tao L, Tan J, Zhang J, Passey DA, et al. Compositional gradients
628 in Gramineae genes. Genome Res 2002;12:851–6.
629 [26] Lobry JR. Asymmetric substitution patterns in the two DNA strands of bacteria. Mol Biol
630 Evol 1996;13:660–5.
631 [27] Wu Z, Lu L, Du J, Yang L, Ren X, Liu B, et al. Comparative analysis of rodent and small
632 mammal viromes to better understand the wildlife origin of emerging infectious diseases.
633 Microbiome 2018;6:178.

634 [28] Pan Y, Zhang D, Yang P, Poon LLM, Wang Q. Viral load of SARS-CoV-2 in clinical
635 samples. Lancet Infect Dis 2020;20:411–2.
636 [29] Wang W, Xu Y, Gao R, Lu R, Han K, Wu G, et al. Detection of SARS-CoV-2 in Different
637 Types of Clinical Specimens. JAMA 2020.
638 [30] Rambaut A, Holmes EC, O'Toole A, Hill V, McCrone JT, Ruis C, et al. A dynamic
639 nomenclature proposal for SARS-CoV-2 lineages to assist genomic epidemiology. Nat
640 Microbiol 2020.
641 [31] Tang X, Wu C, Li X, Song Y, Yao X, Wu X, et al. On the origin and continuing evolution
642 of SARS-CoV-2. National Science Review 2020.
643 [32] Elbe S, Buckland-Merrett G. Data, disease and diplomacy: GISAID's innovative
644 contribution to global health. Glob Chall 2017;1:33–46.
645 [33] Zhou H, Chen X, Hu T, Li J, Song H, Liu Y, et al. A Novel Bat Coronavirus Closely
646 Related to SARS-CoV-2 Contains Natural Insertions at the S1/S2 Cleavage Site of the Spike
647 Protein. Curr Biol 2020;30:2196-203 e3.
648 [34] Zhou P, Yang XL, Wang XG, Hu B, Zhang L, Zhang W, et al. A pneumonia outbreak
649 associated with a new coronavirus of probable bat origin. Nature 2020;579:270–3.
650 [35] Becerra-Flores M, Cardozo T. SARS-CoV-2 viral spike G614 mutation exhibits higher
651 case fatality rate. Int J Clin Pract 2020:e13525.
652 [36] Daniloski Z, Guo X, Sanjana NE. The D614G mutation in SARS-CoV-2 Spike increases
653 transduction of multiple human cell types. bioRxiv 2020:2020.06.14.151357.
654 [37] Korber B, Fischer W, Gnanakaran S, Yoon H, Theiler J, Abfalterer W, et al. Spike
655 mutation pipeline reveals the emergence of a more transmissible form of SARS-CoV-2.
656 bioRxiv 2020:2020.04.29.069054.
657 [38] Zhang L, Jackson CB, Mou H, Ojha A, Rangarajan ES, Izard T, et al. The D614G mutation
658 in the SARS-CoV-2 spike protein reduces S1 shedding and increases infectivity. bioRxiv
659 2020:2020.06.12.148726.
660 [39] Wang M, Fu A, Hu B, Tong Y, Liu R, Gu J, et al. Nanopore target sequencing for accurate
661 and comprehensive detection of SARS-CoV-2 and other respiratory viruses. medRxiv
662 2020:2020.03.04.20029538.
663 [40] Teymoori-Rad M, Samadizadeh S, Tabarraei A, Moradi A, Shahbaz MB, Tahamtan A.
664 Ten challenging questions about SARS-CoV-2 and COVID-19. Expert Rev Respir Med 2020.
665 [41] Liu Q, Zhao S, Shi C-M, Song S-H, Zhu S, Su Y, et al. Population genetics of SARS-
666 CoV-2: disentangling sampling bias and clustering infections. Genomics Proteomics
667 Bioinformatics 2020;in press.

668 [42] Cotten M, Watson SJ, Kellam P, Al-Rabeeah AA, Makhdoom HQ, Assiri A, et al.
669 Transmission and evolution of the Middle East respiratory syndrome coronavirus in Saudi
670 Arabia: a descriptive genomic study. Lancet 2013;382:1993–2002.
671 [43] Gire SK, Goba A, Andersen KG, Sealfon RSG, Park DJ, Kanneh L, et al. Genomic
672 surveillance elucidates Ebola virus origin and transmission during the 2014 outbreak. Science
673 2014;345:1369–72.
674 [44] Lemey P, Suchard M, Rambaut A. Reconstructing the initial global spread of a human
675 influenza pandemic: A Bayesian spatial-temporal model for the global spread of H1N1pdm.
676 PLoS Curr 2009;1:RRN1031.
677 [45] Smith GJD, Vijaykrishna D, Bahl J, Lycett SJ, Worobey M, Pybus OG, et al. Origins and
678 evolutionary genomics of the 2009 swine-origin H1N1 influenza A epidemic. Nature
679 2009;459:1122–5.
680 [46] Yu W-B, Tang G-D, Zhang L, Corlett RT. Decoding the evolution and transmissions of
681 the novel pneumonia coronavirus (SARS-CoV-2 / HCoV-19) using whole genomic data. Zool
682 Res 2020;41:247–57.
683 [47] Sanders W, Fritch EJ, Madden EA, Graham RL, Vincent HA, Heise MT, et al.
684 Comparative analysis of coronavirus genomic RNA structure reveals conservation in SARS-
685 like coronaviruses. bioRxiv 2020:2020.06.15.153197.
686 [48] National Genomics Data Center M, Partners. Database Resources of the National
687 Genomics Data Center in 2020. Nucleic Acids Res 2020;48:D24–D33.
688 [49] Wang B, Liu F, Zhang EC, Wo CL, Chen J, Qian PY, et al. The China National GeneBank
689 horizontal line owned by all, completed by all and shared by all. Hereditas(Beijing)
690 2019;41:761-72.
691 [50] Sayers EW, Cavanaugh M, Clark K, Ostell J, Pruitt KD, Karsch-Mizrachi I. GenBank.
692 Nucleic Acids Res 2020;48:D84–D6.
693 [51] Wu L, Sun Q, Desmeth P, Sugawara H, Xu Z, McCluskey K, et al. World data centre for
694 microorganisms: an information infrastructure to explore and utilize preserved microbial
695 strains worldwide. Nucleic Acids Res 2017;45:D611–D8.
696 [52] Edgar RC. MUSCLE: multiple sequence alignment with high accuracy and high
697 throughput. Nucleic Acids Res 2004;32:1792–7.
698 [53] Kumar S, Stecher G, Li M, Knyaz C, Tamura K. MEGA X: Molecular Evolutionary
699 Genetics Analysis across Computing Platforms. Mol Biol Evol 2018;35:1547-9.
700 [54] Marra MA, Jones SJ, Astell CR, Holt RA, Brooks-Wilson A, Butterfield YS, et al. The
701 Genome sequence of the SARS-associated coronavirus. Science 2003;300:1399-404.

[55] McLaren W, Gil L, Hunt SE, Riat HS, Ritchie GRS, Thormann A, et al. The Ensembl Variant Effect Predictor. Genome Biol 2016;17:122.
[56] Price MN, Dehal PS, Arkin AP. FastTree 2--approximately maximum-likelihood trees for large alignments. PLoS One 2010;5:e9490.
[57] Letunic I, Bork P. Interactive Tree Of Life (iTOL) v4: recent updates and new developments. Nucleic Acids Res 2019;47:W256–W9.
[58] Schliep KP. phangorn: phylogenetic analysis in R. Bioinformatics 2011;27:592–3.
[59] Yu G. Using ggtree to Visualize Data on Tree-Like Structures. Curr Protoc Bioinformatics 2020;69:e96.

Figures

Figure 1 A display of genome compositional dynamics of SARS-CoV-2 and related CoVs

A. The complete genome sequence of SARS-CoV-2 (NC_045512.2), including both structural and non-structural components. **B.** We use a 300-nt sliding window with a 21-nt step to show dynamic changes of genome G+C, purine, GC1 to GC3, and GC skew (G-C/G+C) contents over the entire genomes. **C.** A similar procedure as described above is applied to individual ORFs and proteins. Note that the GC skews are not uniform over the genome length and the observation suggests possible recent recombination among closely related CoVs.

Figure 2 Nucleobase contents of genomes and subgenomes of SARS-CoV-2 and related CoVs

A. A schematic phylogenetic tree is used to cluster genome sequences and compositional variables (15 CoVs genome sequences, from top to bottom, are: hsa-betaCoV-HKU1, hsa-betaCoV-OC43, ave-gamaCoV, mga-gamaCoV, smu-alphaCoV-WS, hsa-alphaCoV-229E, hsa-alphaCoV-NL63, taf-alphaCoV-NL63, MERS-CoV, cdr-betaCoV-B73, SARS-CoV, pla-betaCoV-SZ3, mja-betaCoV-P4L, SARS-CoV-2, and raf-betaCoV-RaTG13). These compositional variables include GC contents at three codon positions (codon positions 1, 2, and 3 are denoted as GC1, GC2, and GC3) and single nucleotide contents at three codon positions (A1, A2, A3; U1, U2, U3; G1, G2, G3; and C1, C2, C3). Nucleotides are labeled in different shapes: purines, triangles; pyrimidines, open circles. A and U or G and C are colored blue or red, respectively. It becomes obvious that the two closely-related CoV genomes to SARS-CoV-2, the reported bat (raf-betaCoV-RaTG13) and the pangolin (mja-betaCoV-P4L) have very similar codon G+C content as well as base contents. The cp1 (codon position 1) base content appears most characteristic of balanced purine content of SARS-CoV-2 and its close

735 relatives. The cp2 (codon position 2) base content of SARS-CoV-2 and all other CoVs has
736 higher and relatively balanced A+U content. The older human CoVs have either lowest or
737 higher G+C content and unbalanced purine contents. Note that G+C contents in three codon
738 positions are labeled differently from those of single nucleotide contents in color codes. G+C
739 content represents a single measure but single nucleotide contents demonstrate trends of all
740 four nucleotides. **B.** The G+C and single nucleotide contents at different codon positions of
741 complete genomes and subgenomes of SARS-CoV-2, SARS-CoV, mja-betaCoV-P4L, and raf-
742 betaCoV-RaTG13 are displayed to illustrate the driving force for G+C content decrease toward
743 3' end of the genome, which is rather a result of, in terms of mechanism, the increased U
744 content and C-to-U permutation. The negative gradient of U is also obvious from the 5' end to
745 the 3' end.

746 **Figure 3 Mutation spectra of SARS-CoV-2 in a context of G+C contents and codon**
747 **positions**

748 **A.** The SARS-CoV-2 mutation spectrum is composed of 12 permutations and they are divided
749 by codon positions among all mutations. C-to-U (CU), U-to-C (UC), A-to-G (AG), G-to-A
750 (GA), and G-to-U (GU), are always dominant due to two principles; one is that the first four
751 permutations occur when positive-sense genome is synthesized, and the other is that a G-by-A
752 replacement is always preferred by RTCs so that G-to-U permutation as the most dominant
753 occurring when the antigenome serves as a template. **B.** C-to-U permutations at cp3 diminish
754 among non-synonymous mutations and this phenomenon indicates that most protein
755 composition relevant variations are cp1 and cp2 variations. The remaining non-synonymous
756 mutations in G-to-U (GU) permutation may be a result of biased strand synthesis. **C.** Displays
757 of permutation-to-codon changes among non-synonymous mutations. The codon table is
758 divided into two halves: the pro-diversity half (blue) whose cp3 is sensitive to transitional
759 change and the pro-robust half (purple) whose cp3 position is insensitive to any change. Two
760 examples, C-to-U (1051 in counts) and A-to-G (314 in counts) permutations are shown here.
761 When a codon has a C-to-U change, the codon position varies, results of such changes relative
762 to codon positions are summarized on both sides of the codon flow chart. Note that cp1 and
763 cp2 changes appear more than those of cp3. The ratio between codons of pro-robust half and
764 pro-diversity half is displayed on each bar. **D.** All permutations are plotted against the reference
765 genome sequence to show how changes are related to amino acids. In the molecular weight
766 index, most cp1 and cp2 changes are most obvious, showing an increasing trend. In the
767 hydrophobicity index, most cp1 and cp2 changes increase toward less hydrophobicity.

768 **Figure 4 Sequence-variation-based phylogenies of SARS-CoV-2**

769 **A.** CoV genomes are divided into clades and clade clusters based on high-frequency mutations
770 among the genome sequences. The shared variations are excellent indicators for shared
771 ancestors and those between clusters (blue half parentheses) and within clusters (red half
772 parentheses) are labeled with positions and nucleotide variations that are all referenced to the
773 SARS-CoV-2 genome (NC_045512.2), its positions, and relative frequencies (thin vertical
774 bars). The dates when each clade started are also indicated. **B.** The current collection shows 9
775 clades (C01 to C09) in three clusters (S, L and G). An unrooted phylogenic tree of the clades
776 and clusters (color-coded), the tree scale is 0.01.

777 **Figure 5 Mutation spectrum and composition dynamics among 9 SARS-CoV-2 clades**

778 **A.** Plots showing permutation variation of each clade. Aside from the 5 dominant permutations,
779 A-to-C (R2 permutation), U-to-G (R2 permutation) and A-to-U (R12 permutation) changes
780 appear also significant; such an increase in proportion of R2 and R12 permutations often
781 indicates copy number (synthesis) bias between the two strands. **B.** When permutations are
782 grouped based on structure-conformation model (Figure S5) into tight and loose groups (a four-
783 parameter model), their trends of changes become obvious. The R-tight discourages A-by-G
784 replacement but encourages C-by-U replacement when the genome is replicated. The loose
785 statuses, regardless R-loose or Y-loose, place no pressure on permutation variability. **C**. Violin
786 plots showing the G+C content among clades. **D**. Violin plots showing the purine content
787 among the clades. C08 and C09 have been drifting both contents toward lower ends. C03 has
788 also been drifting in a greater extent of its purine content and a lesser extent of its G+C content,
789 comparatively. **E.** The mean (solid circles) and median (solid triangles) of G+C and purine
790 contents among clades. The same three more expressive clades, as seen in (**C**) and (**D**), are
791 indeed obvious (inset). **F.** The compositional dynamics of cp3 nucleotides that are less selected
792 and with a stringent cutoff value (> or =5). **G.** Composition distributions based on major alleles,
793 at frequencies equal or greater than 0.01 to emphasize the effect from selection. **H**.
794 Composition distributions based on major alleles at frequencies equal or greater than 0.05. **I**.
795 Composition distributions based on major alleles at frequencies equal or greater than 0.1.

796 **Figure 6 Within-clade permutation variations are excellent indicators of functional**
797 **mutations**

798 **A.** An example of permutation shifting of clade C02 and among its subclades. The number of
799 SARS-CoV-2 genomes is indicated in the parentheses. The clear trends are two-fold. First,
800 decreased C-to-U permutation is coupled with increased A-to-G and decreased G-to-U
801 permutations. Second, A-to-U permutation is also increased as expected based on the model
802 shown in Figure S5. These trends pf permutation changes suggest irrelevant to the ratio of

strand-biased synthesis (positive sense vs negative sense) but possible structural and/or conformational variation in the RTCs. (**B**) – (**F**) show within-clade permutation changes of C02, C04, C03, C05 and C07. In each display, the first column of the x-axis shows the proportion of permutations calculated for each clade. Two opposite trends of permutation variations are seen between C03 and C04, and C07 has a rather wavy pattern.

Supplementary material

Supplementary Figure S1 A display of genome compositional dynamics of SARS-CoV, MERS-CoV and their within-population CoVs

We use a 300-bp sliding window with a 21-bp step to show dynamic changes of genome G+C, purine, GC1 to GC3, and GC skew (G-C/G+C) contents. The complete genome sequences and data sources are listed in Table S1.

Supplementary Figure S2

A. G+C and purine content plot to show how these contents distribute among human CoVs. Note that all older human CoVs are drifted toward lower G+C and purine contents, and this phenomenon indicates lower selection pressure or insensitivity on composition changes. Full names of the human CoVs are listed in the legend of Figure 2. **B.** A genetic code table to show how nucleotide permutations are related to codons. The table is divided into two halves (colored and uncolored backgrounds) and cp1 and cp2 relative to their permutations sensitivity and changes are indicated with half parentheses with color-coding: C-to-U|U-to-C and A-to-G|G-to-A, red; G-to-U|U-to-G and A-to-C and C-to-U, blue; and A-to-U|U-to-A and G-to-C|C-to-G, green. Note that cp1 and cp2 are sensitive to column and row codon swaps, respectively. Cp3 is in a unique position where only half of the codons are sensitive to its changes, and the other half is so organized that some codons are more permissive than others.

Supplementary Figure S3 Mutation spectra of SARS-CoV-2 in a context of codon positions

A. MERS-CoV and SARS-CoV mutation spectra are composed of 12 permutations and they are divided by codon positions. C-to-U (CU) permutations are always as dominant as what SARS-CoV-2 shows. The mutation counts are partitioned into synonymous and non-synonymous mutations. **B.** C-to-U permutations at cp3 diminish among non-synonymous mutations and this phenomenon indicates that most protein composition relevant variations are cp1 and cp2 variations. Note that all older human CoVs are drifted toward lower G+C and purine contents, and this phenomenon indicates lower selection or insensitivity on composition

836 changes. Full names of the human CoVs are listed in the legend of Figure 2. Mutation counts
837 are calculated from non-synonymous mutations. **C.** Displays of permutation-to-codon changes
838 among non-synonymous mutations. The permutations showed here contain U-to-C, G-to-A,
839 G-to-U, C-to-A, U-to-G, A-to-C, A-to-U, G-to-C, U-to-A and C-to-G.

840 **Supplementary Figure S4 High-frequency within-clade mutations**

841 Signature site information and frequency table of star mutations in each clade, with a neighbor-
842 joining tree based on the frequency data in the table.

843 **Supplementary Figure S5**

844 This table illustrates how 12 permutations are related to G+C and purine contents and the subtle
845 RTC specificity of CoVs. Mutations occur when the positive-sense RNA genome (R1,
846 mutation happens when the negative-sense genome is synthesized) or its negative-sense
847 subgenomes are synthesized (R2). The G+C content insensitive permutations occur after two
848 syntheses (R12). CU and A-to-G (AG) are preferred when RTC is in a status that encourages
849 a large-to-small substrate exchange in a higher ratio than the opposite, small-to-large substrate
850 exchange. We term this preferred exchange as "tight" status. This status is also divided into R-
851 tight (R, purine; to indicate that the mechanism is an A-by-G replacement) and Y-tight (Y,
852 pyrimidine; to indicate that the mechanism is a C-by-U replacement). When an exchange of
853 substrate happens from small-to-large, it is referred as a "loose" status that is also divided into
854 two, R-loose and Y-loose. Note that some permutations are not sensitive to G+C and purine
855 contents but others are sensitive. Arrow-headed dashed lines connect R1 permutation to R12
856 permutations, and note that cross-column relationship is rather striking, which re-routes some
857 structural principles, which navigates mutation forces on one hand and leaves room for
858 selection to work on, on the other hand.

859 **Supplementary Figure S6 Within-clade permutation variations are excellent indicators**
860 **of functional mutations**

861 (**A**) – (**D**) show within-clade permutation changes of C06, C08, C09 and C01.

862

863 **Supplementary Table S1 The mutation counts in each clade and cluster**

864 **Supplementary Table S2 The proportion of permutations in each clade and clusters**
865 **based on different genomic regions**

866 **Supplementary Table S3 Selected CoV genome sequences used for this study**

867 **Supplementary Table S4 The SARS-Cov-2 mutation table on coding region (based on**
868 **data on June 12th 2020)**

869 **Supplementary Table S5 The proportion of permutations in each clade and their**
870 **subclades**

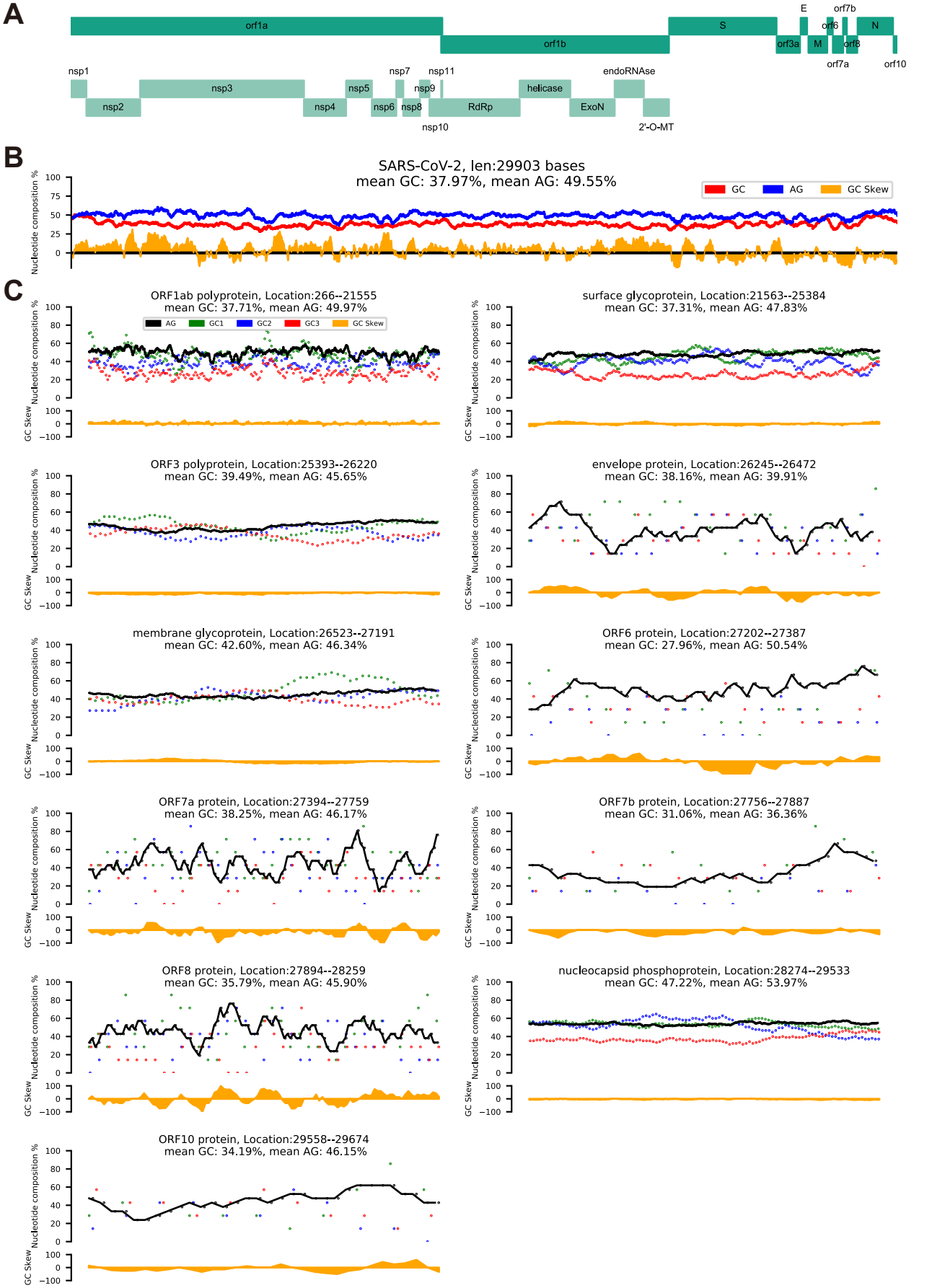
A
orf1a
orf1b
S
E
orf7b
orf6
N
orf3a
M
orf8
orf7a
orf10
nsp1
nsp2
nsp3
nsp4
nsp5
nsp6
nsp7
nsp8
nsp9
nsp10
nsp11
RdRp
helicase
ExoN
endoRNAse
2'-O-MT
B
SARS-CoV-2, len:29903 bases
mean GC: 37.97%, mean AG: 49.55%
GC
AG
GC Skew
Nucleotide composition %
C
ORF1ab polyprotein, Location:266--21555
mean GC: 37.71%, mean AG: 49.97%
AG
GC1
GC2
GC3
GC Skew
surface glycoprotein, Location:21563--25384
mean GC: 37.31%, mean AG: 47.83%
ORF3 polyprotein, Location:25393--26220
mean GC: 39.49%, mean AG: 45.65%
envelope protein, Location:26245--26472
mean GC: 38.16%, mean AG: 39.91%
membrane glycoprotein, Location:26523--27191
mean GC: 42.60%, mean AG: 46.34%
ORF6 protein, Location:27202--27387
mean GC: 27.96%, mean AG: 50.54%
ORF7a protein, Location:27394--27759
mean GC: 38.25%, mean AG: 46.17%
ORF7b protein, Location:27756--27887
mean GC: 31.06%, mean AG: 36.36%
ORF8 protein, Location:27894--28259
mean GC: 35.79%, mean AG: 45.90%
nucleocapsid phosphoprotein, Location:28274--29533
mean GC: 47.22%, mean AG: 53.97%
ORF10 protein, Location:29558--29674
mean GC: 34.19%, mean AG: 46.15%
GC Skew

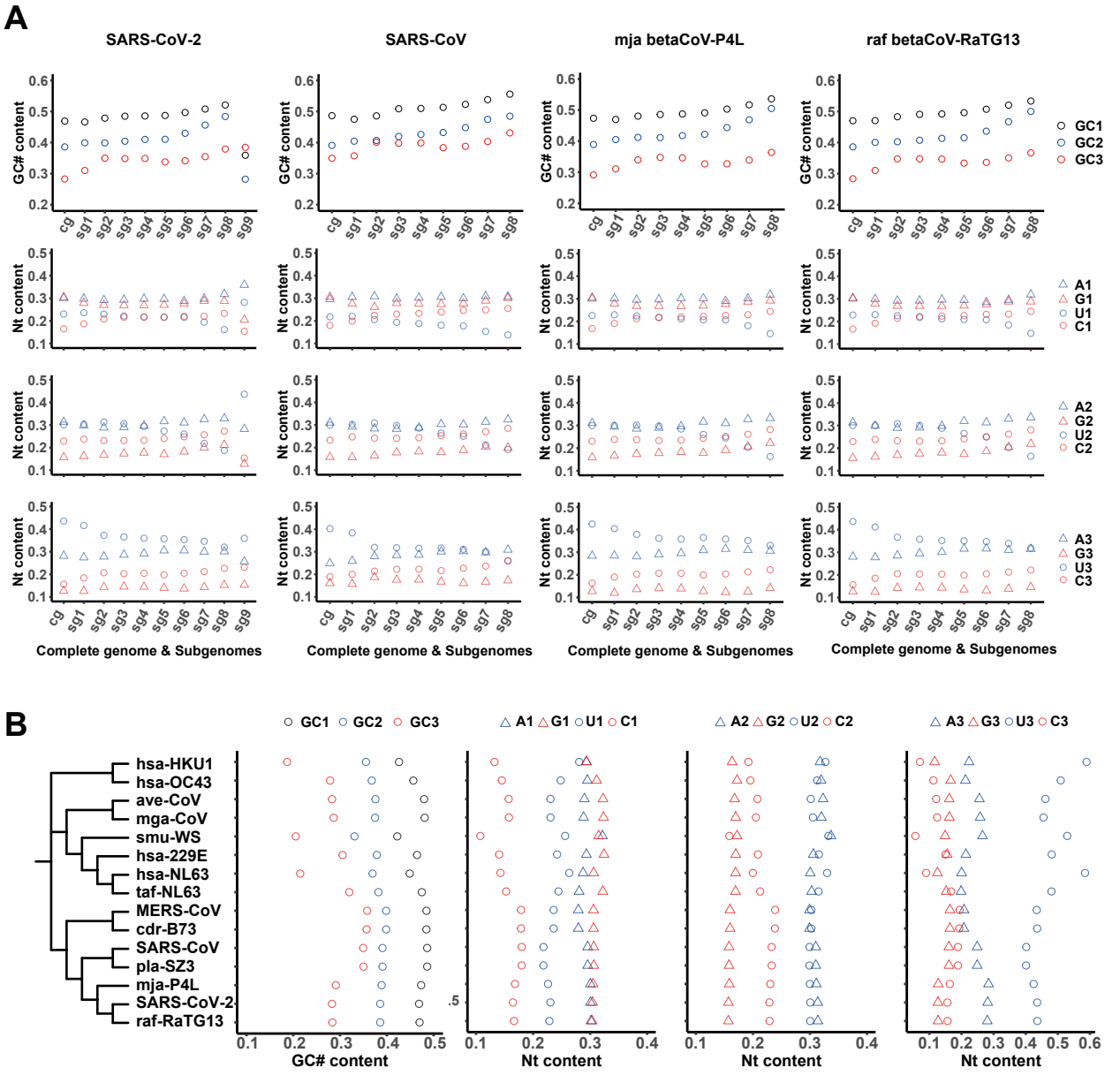
A
SARS-CoV-2
SARS-CoV
mja betaCoV-P4L
raf betaCoV-RaTG13
GC# content
Nt content
cg
sg1
sg2
sg3
sg4
sg5
sg6
sg7
sg8
sg9
GC1
GC2
GC3
A1
G1
U1
C1
A2
G2
U2
C2
A3
G3
U3
C3
Complete genome & Subgenomes
B
hsa-HKU1
hsa-OC43
ave-CoV
mga-CoV
smu-WS
hsa-229E
hsa-NL63
taf-NL63
MERS-CoV
cdr-B73
SARS-CoV
pla-SZ3
mja-P4L
SARS-CoV-2
raf-RaTG13
GC# content
Nt content

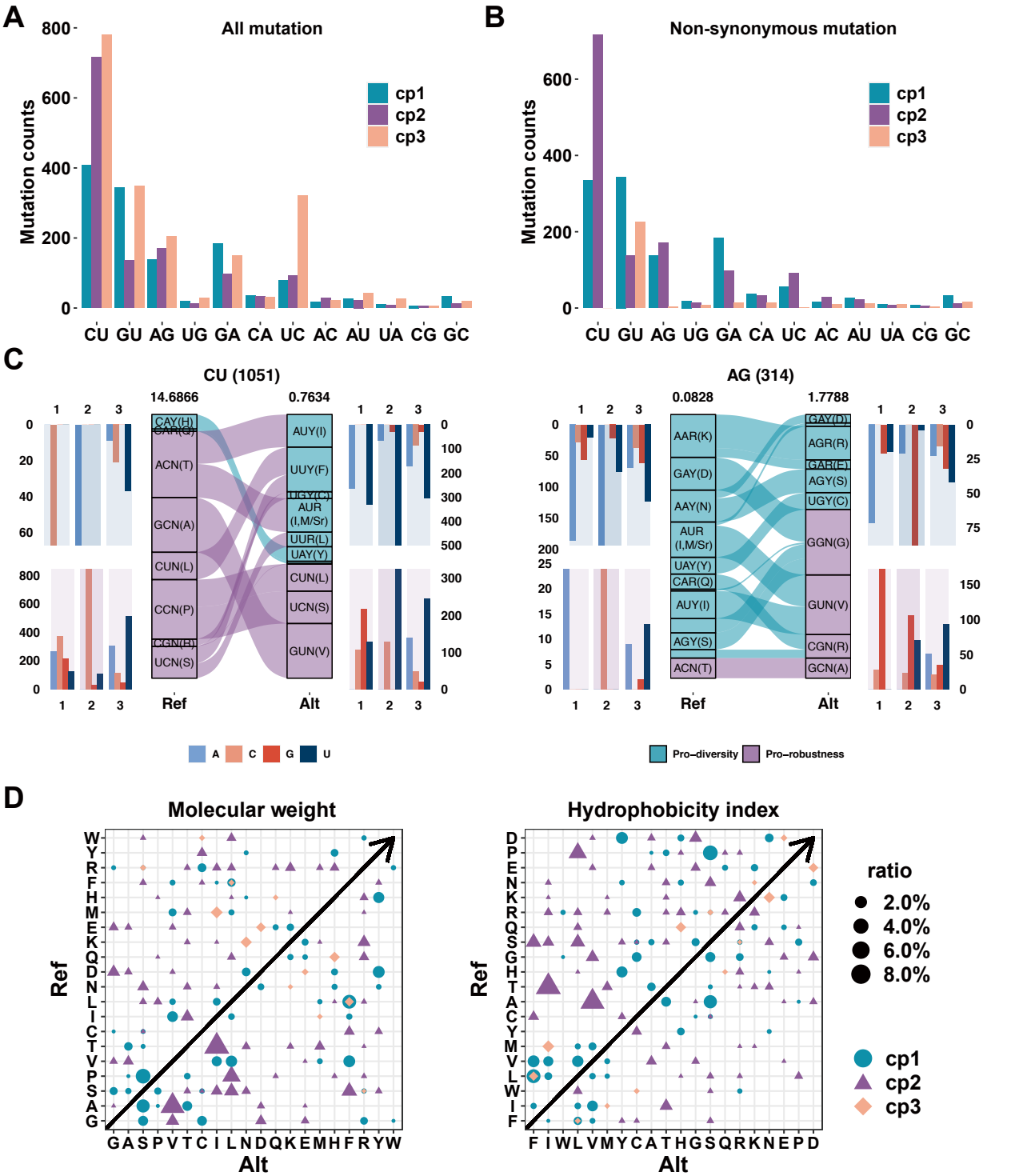
A
All mutation
Mutation counts
cp1
cp2
cp3
CU GU AG UG GA CA UC AC AU UA CG GC
B
Non-synonymous mutation
Mutation counts
C
CU (1051)
14.6866
0.7634
AG (314)
0.0828
1.7788
Ref
Alt
A C G U
Pro−diversity
Pro−robustness
D
Molecular weight
Hydrophobicity index
Ref
Alt
ratio
2.0%
4.0%
6.0%
8.0%
cp1
cp2
cp3

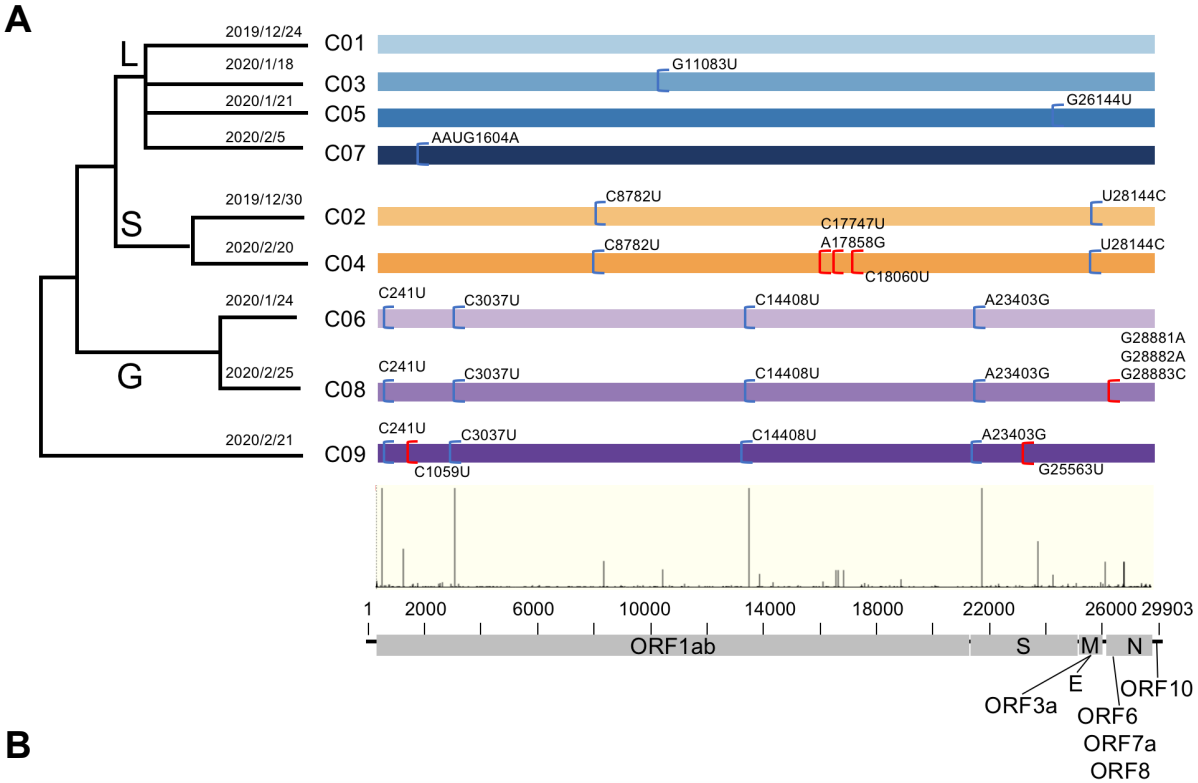
A
L
S
G
2019/12/24
2020/1/18
2020/1/21
2020/2/5
2019/12/30
2020/2/20
2020/1/24
2020/2/25
2020/2/21
C01
C03
C05
C07
C02
C04
C06
C08
C09
G11083U
G26144U
AAUG1604A
C8782U
U28144C
C17747U
A17858G
C18060U
C241U
C3037U
C14408U
A23403G
G28881A
G28882A
G28883C
C1059U
G25563U
1
2000
6000
10000
14000
18000
22000
26000
29903
ORF1ab
S
M
N
E
ORF3a
ORF6
ORF7a
ORF8
ORF10

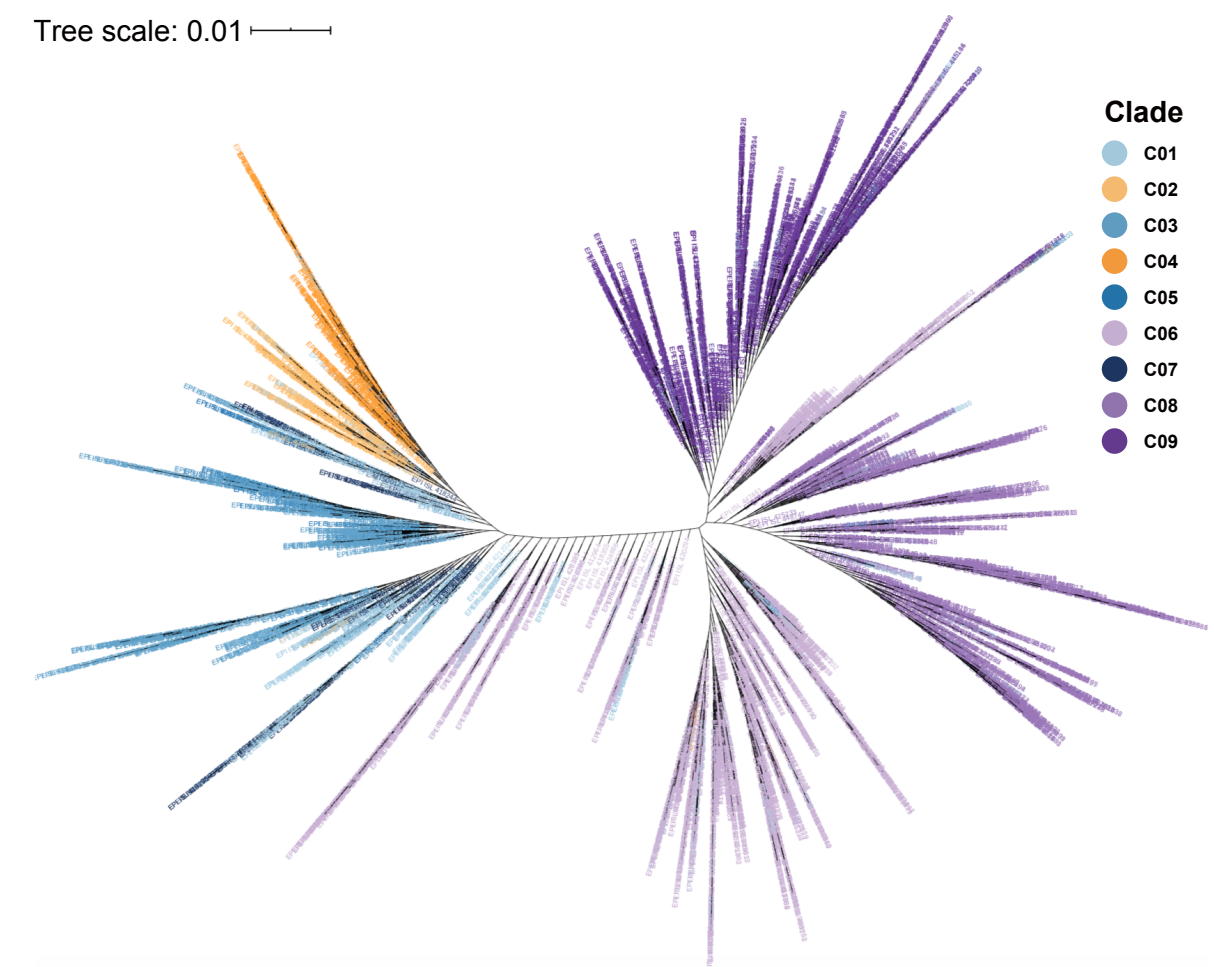
B
Tree scale: 0.01
Clade
C01
C02
C03
C04
C05
C06
C07
C08
C09

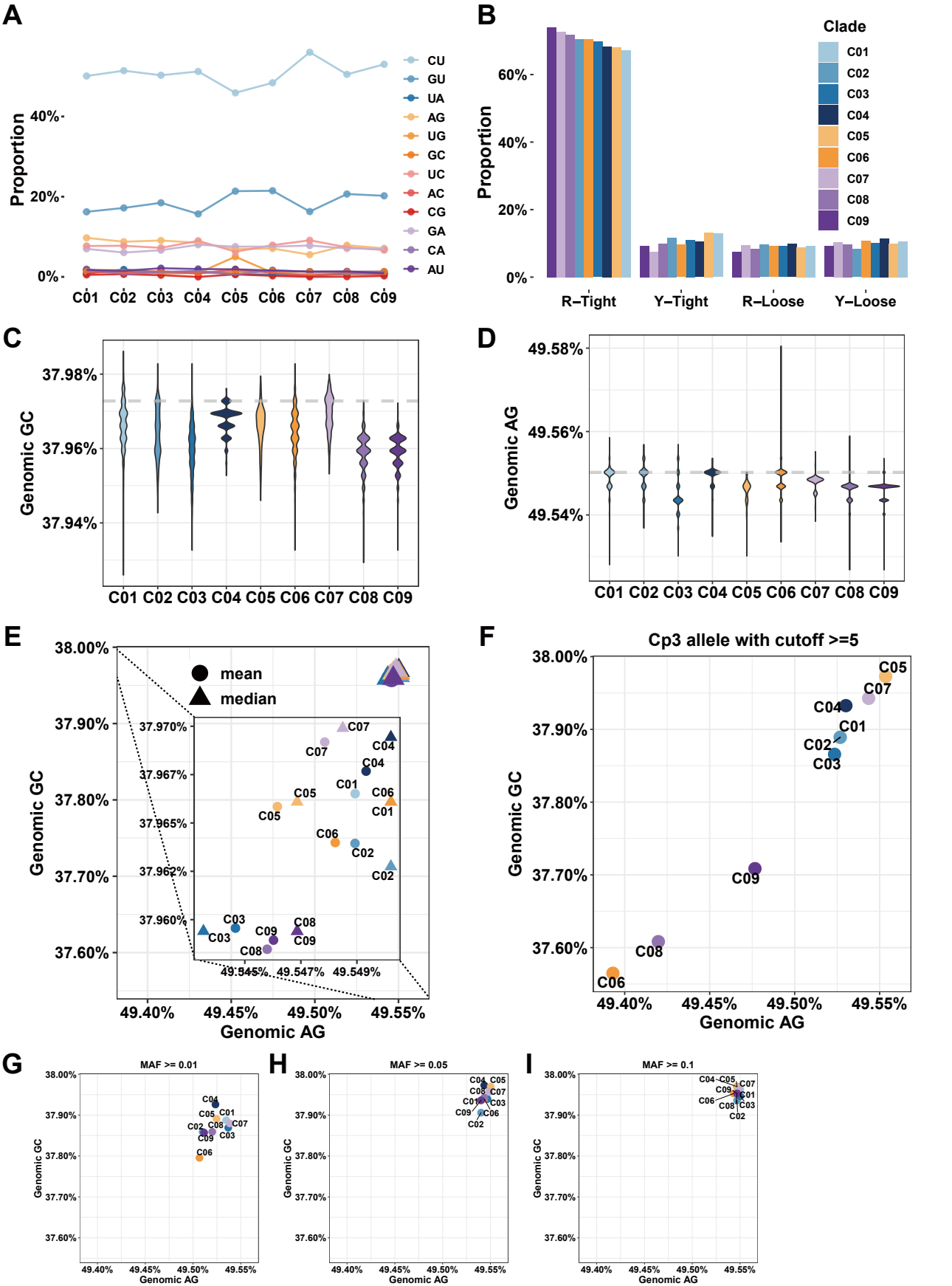
A
Proportion
40%
20%
0%
C01 C02 C03 C04 C05 C06 C07 C08 C09
CU
GU
UA
AG
UG
GC
UC
AC
CG
GA
CA
AU
B
Clade
C01
C02
C03
C04
C05
C06
C07
C08
C09
Proportion
60%
40%
20%
0%
R−Tight
Y−Tight
R−Loose
Y−Loose
C
Genomic GC
37.98%
37.96%
37.94%
C01 C02 C03 C04 C05 C06 C07 C08 C09
D
Genomic AG
49.58%
49.56%
49.54%
C01 C02 C03 C04 C05 C06 C07 C08 C09
E
mean
median
Genomic GC
38.00%
37.90%
37.80%
37.70%
37.60%
37.970%
37.967%
37.965%
37.962%
37.960%
49.545%
49.547%
49.549%
49.40%
49.45%
49.50%
49.55%
Genomic AG
F
Cp3 allele with cutoff >=5
Genomic GC
38.00%
37.90%
37.80%
37.70%
37.60%
C05
C07
C04
C01
C02
C03
C09
C08
C06
49.40%
49.45%
49.50%
49.55%
Genomic AG
G
MAF >= 0.01
Genomic GC
Genomic AG
H
MAF >= 0.05
Genomic GC
Genomic AG
I
MAF >= 0.1
Genomic GC
Genomic AG

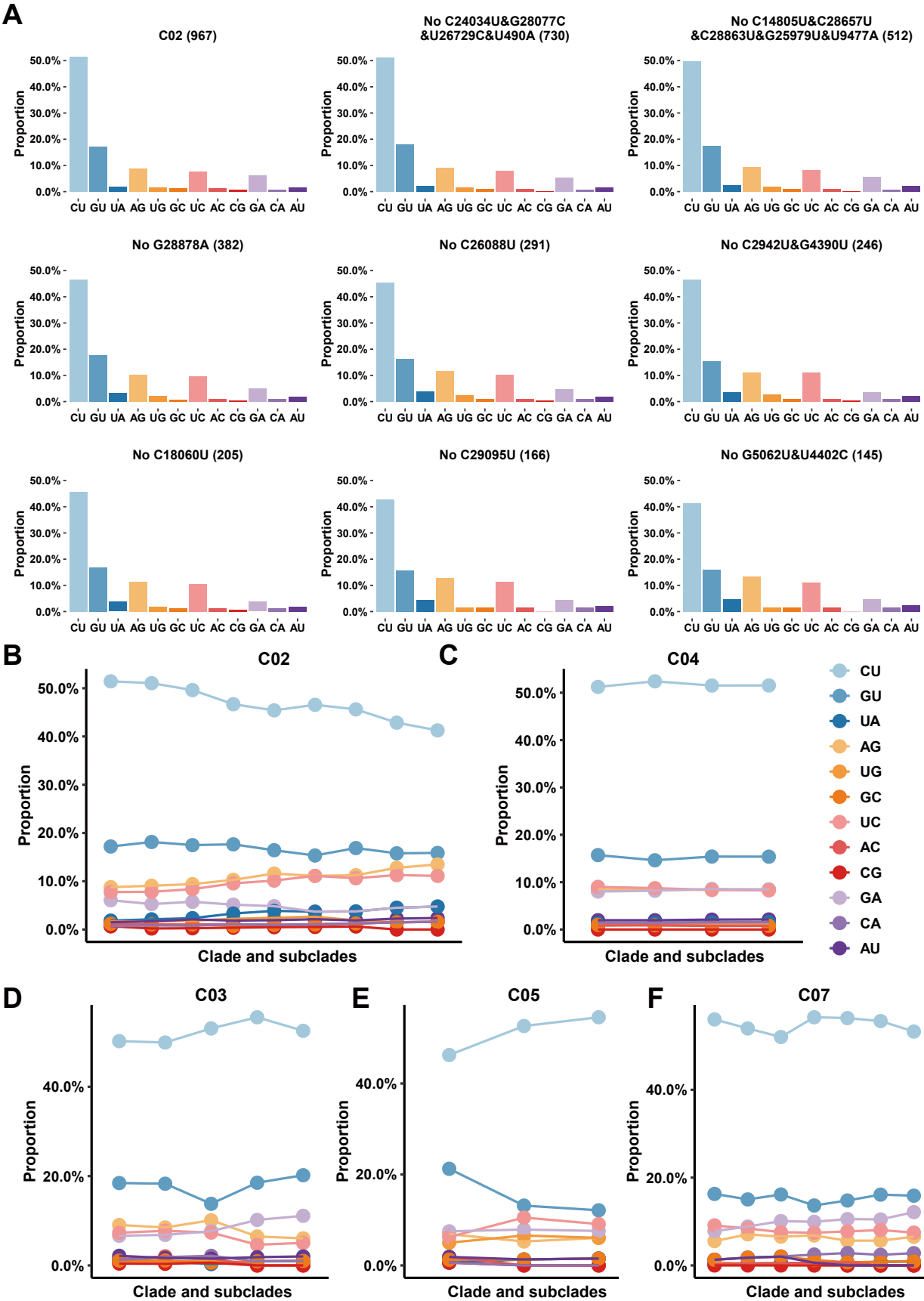
A
C02 (967)
No C24034U&G28077C &U26729C&U490A (730)
No C14805U&C28657U &C28863U&G25979U&U9477A (512)
No G28878A (382)
No C26088U (291)
No C2942U&G4390U (246)
No C18060U (205)
No C29095U (166)
No G5062U&U4402C (145)
Proportion
50.0%
40.0%
30.0%
20.0%
10.0%
0.0%
CU GU UA AG UG GC UC AC CG GA CA AU
B
C02
C
C04
D
C03
E
C05
F
C07
Clade and subclades
CU
GU
UA
AG
UG
GC
UC
AC
CG
GA
CA
AU